Journal of Membrane Science 619 (2021) 118756

Contents lists available at ScienceDirect

Journal of Membrane Science

journal homepage: http://www.elsevier.com/locate/memsci

Sterilization of polypropylene membranes of facepiece respirators by ionizing radiation

Luka Pirker [a,1], Anja Pogačnik Krajnc [a,1], Jan Malec [a,1], Vladimir Radulović [a], Anton Gradišek [a], Andreja Jelen [a], Maja Remškar [a], Igor B. Mekjavić [a], Janez Kovač [a], Miran Mozetič [a], Luka Snoj [a,b,*]

[a] Jožef Stefan Institute, Jamova Cesta 39, 1000, Ljubljana, Slovenia
[b] University of Ljubljana, Faculty of Mathematics and Physics, Jadranska Ulica 19, 1000, Ljubljana, Slovenia

ARTICLE INFO

Keywords:
Respirators
COVID-19
SARS-CoV-2
Sterilization
Personal protection equipment
Ionizing radiation
Polypropylene membrane

ABSTRACT

ABSTRACT: Ionizing radiation has been identified as an option for sterilization of disposable filtering facepiece respirators in situations where the production of the respirators cannot keep up with demand. Gamma radiation and high energy electrons penetrate deeply into the material and can be used to sterilize large batches of masks within a short time period. In relation to reports that sterilization by ionizing radiation reduces filtration efficiency of polypropylene membrane filters on account of static charge loss, we have demonstrated that both gamma and electron beam irradiation can be used for sterilization, provided that the respirators are recharged afterwards.

1. Introduction

As in the previous SARS epidemic in 2003, the current COVID-19 pandemic has also rapidly depleted the global supply of disposable filtering facepiece respirators (FFRs). The production of new FFR cannot keep up with the demand, leaving health professionals and other workers in high-risk environments without adequate protection. Even though the FFRs are designed for single use, the pandemic crisis made it necessary to seek for emergency alternatives. Recycling of single use personal protective equipment is one such option, but requires appropriate and efficient sterilization procedures. After sterilization the FFRs must still provide adequate protection according to the criteria of the used standard.

Several conventional sterilization methods have recently been tested on FFRs, with vastly different success [1]. Dry heating below 100 °C, steam treatment, ethylene oxide and vaporized hydrogen peroxide were reported to be efficient by preserving the filtration characteristics of FFRs, but with some shortcomings such as lengthy procedures and low throughput [2]. Although UV-C irradiation does not affect the filtration efficiency, there are concerns that its limited penetration in the material does not offer complete in-depth sterilization, while sterilization using liquids (i.e. alcohol, chlorine-based solutions, or soap) removes the static charge, rendering the masks less efficient [3, p. 9]. Recharging the mask after the sterilization with alcohol improves the filtration efficiency to some extent, but it did not return to previous values [4]. Regardless of the sterilization strategy, it is necessary that the method preserves the structural integrity and shape of the mask, in addition to preserving the filtering efficiency. This excludes sterilization methods such as using a microwave oven, which melts mask components. Reusing the respirators after several days is in principle possible, as the SARS-CoV-2 virus (which causes the COVID-19 disease) is deactivated in that time, however, other pathogens may remain [5]. There have been some attempts at using ionizing radiation for sterilization, either gamma rays or electron beam, which are widely used for sterilization of medical equipment on a large scale [6–8]. A dose of 20 kGy resulted in a significant drop of the filtration efficiency, which was attributed to the electric discharge of the filter material of the masks. At present, all studies summarily dismiss the use of ionizing radiation as a promising sterilization option.

According to literature [9] there are five basic particle removal mechanisms. While large particles are mostly caught by the dense mesh of fibres due to interception, impact, or the settling mechanism, particles

* Corresponding author. Jožef Stefan Institute, Jamova cesta 39, 1000 Ljubljana, Slovenia.
E-mail address: luka.snoj@ijs.si (L. Snoj).
[1] L.P., A.P.K and J.M. contributed equally.

https://doi.org/10.1016/j.memsci.2020.118756
Received 14 July 2020; Received in revised form 28 August 2020; Accepted 31 August 2020
Available online 1 October 2020

below 500 nm in size, which also includes viruses with sizes between 50 nm and 200 nm [10], are mostly removed from the inspired air in the mask through electrostatic attraction and diffusion. The static charge, induced either by the corona discharge process [11], additives with varying electrostatic potentials, or by the dipolar nature of the fibres, creates a non-uniform electrical field that imposes a force on the particles which have a net charge or an induced dipole. These forces then retard the progress of the particles, increasing the probability that they impact a fibre due to diffusion and/or directly attract them to the surface of the fibre. Such fibres, called electrets, are not used only in modern FFRs, but also in other applications, such as filters, vacuum cleaners, dust collectors, etc. By irradiating electrets with ionizing radiation, ions and/or electrons are produced in the surrounding gas and are attracted to the electret fibres and reduce the surface charge. Electrons and/or electron holes, which are produced inside the electret during the irradiation, also contribute to the reduction of the surface charge [12,13]. Polypropylene, which is usually used in FFRs, obtains its surface charge during the melt-blowing or melt-spinning process due to the trapping of charge carriers at defects during the manufacturing process [14,15]. Alternatively, surface charge can be applied on finished respirators, commonly with the corona-discharge method [16]. Corona-discharge is an electrical discharge, which ionizes surrounding air around highly charged conductors. The unfortunate similarity of the name of the method ("corona"), with the corona virus is coincidental. Although polypropylene is considered as a nonpolar polymer, a small dipole moment was observed [17] which is however too small to contribute to the filtration efficiency.

In this study we investigated the sterilization options using gamma rays and high energy electrons as well as the relation between the irradiation, particle removal efficiency (PRE) and surface potential on the respirators. In addition, structural changes in FFRs were examined after irradiation with scanning electron microscopy (SEM) and dynamical mechanical analysis (DMA), while possible chemical changes were analyzed with X-ray photoelectron spectroscopy (XPS) and Raman spectroscopy.

The aim of the present study was to investigate whether the FFRs structural integrity and filtering efficiency can be maintained after sterilization with ionizing radiation. It is important to note that we have not studied the process of sterilization itself but irradiated the FFRs to typical doses for sterilization, i.e. around 20 kGy [18].

2. Experimental

2.1. Sample preparation

3M Aura disposable respirator with a valve FFP3 mask and Shenzhen Jingcai Gonginrien Managmen et Co. Ltd. KN95/FFP2 ear face mask, both manufactured according to the EN 149:2001+A1:2009 standard [19]. Pieces of filtration material of 4 cm × 4 cm were cut out of FFRs to fit the inside the TRIGA Mark II Triangular Irradiation Channel where the samples were exposed to gamma-ray radiation. The same method was used when preparing the samples for electron beam irradiation. Each filter was packaged into an airtight bag to prevent any contamination. Special care was taken not to bend the filter or cause any other damage that would result in a reduced filtration efficiency, decreased surface charge and altered mechanical properties.

2.2. Particle removal efficiency

Each filter was placed in a special holder, which prevented any leakages and ensured that the surface exposed to the particulate matter was in all cases the same. The nanoparticle total concentration (TC) and time-dependant size distribution was measured with a Scanning Mobility Particle Sizer (SMPS model 3080 L85; TSI Co., Shoreview, MN, USA) equipped with a desiccator, soft X-ray neutralizer, long differential mobility analyzer (DMA), and a water condensation particle counter (WCPC; model 3785; TSI). The electrical mobility diameter of counted nanoparticles was from 13 nm to 572.5 nm. The air flow at the inlet of the SMPS was 4.1 l/min. The aerosol standard powder ISO 12103-1 A1 was dispersed in the sampling chamber during the measurements with a Topas SAG 410 aerosol generator. The standard powder is without surface charge, which was measured with the method described in section 2.9.

Before each measurement, the test chamber was injected with aerosol particles for 30 min, so that stationary conditions were obtained. The particle size distribution inside an empty chamber under stationary conditions is shown in Fig. 12S–A. The peak of the size distribution of aerosol particles is between 40 nm and 50 nm. The time evolution of the total concentration during a measurement is shown in Fig. 12S–B. Before the test chamber is opened, the TC is almost constant, which shows a high stability of the system. The particle removal efficiency (PRE) is defined in equation 1 in the supporting information.

2.3. Raman spectroscopy

The samples were examined with Micro Raman spectroscopy using a WITec Alpha 300 RS scanning confocal Raman microscope in back-scattered geometry with a polarized Nd:YAG laser operating at the wavelength of 532 nm. The laser beam was focused through a 20x/0.4 microscope objective. The power of the laser at the sample was approximately 12 mW. Raman spectra were recorded on multiple iPP fibres on different layers.

2.4. SEM

Scanning electron microscopy (SEM) images were obtained with a Helios NanoLab 650 Focused Ion Beam-scanning electron microscope (FIB) or a Jeol JSM-7600F scanning electron microscope. Each sample was coated with approximately 10 nm of gold to prevent charging effects during electron irradiation.

2.5. X-ray photoelectron spectroscopy

X-ray photoelectron spectroscopy (XPS) analysis was carried out on a TFA XPS spectrometer (Physical Electronics inc.). The analyzed area was 0.4 mm in diameter and about 3–5 nm in depth. Sample surface was excited by X-ray radiation from a monochromatic Al source with the photon energy of 1486.6 eV. The spectra were acquired with an energy resolution of about 0.6 eV with an analyzer pass energy of 29 eV.

2.6. Dynamic mechanical analysis

The measurements were performed with the Mettler Toledo DMA/SDTA861^e. The tension experiments were performed at 10 Hz with an amplitude of 20 μm in the temperature range from −30 °C to 80 °C. For each sample the experiment was performed three times. The thickness and the diameter of each sample were measured before the experiment. Before each temperature scan a linearity test was made on each sample to determine the optimal displacement amplitude.

2.7. Gamma irradiation

The Jozef Stefan Institute TRIGA Mark II reactor is a typical TRIGA pool-type research nuclear reactor, cooled by natural convection, with a maximal steady-state thermal power of 250 kW. The reactor is equipped with several irradiation channels, both in-core and ex-core with differing experimental conditions. In shutdown conditions, the reactor is a viable source for irradiations with gamma radiation, due to the fission and activation products contained in the fuel and structural components [20–22]. In this study, we used the Triangular Irradiation Channel (TIC), occupying three fuel element positions in the reactor core, enabling irradiations of samples with a lateral dimension of approximately 50 mm.

The gamma dose delivered to the respirators was controlled by monitoring the dose rate as a function of time during the irradiations, using an absolutely calibrated PTW Farmer ionization chamber. The ionization chamber was irradiated simultaneously with the FFRs. A schematic and optical image of the reactor is shown in Fig. 13S.

2.8. Electron beam irradiation

The electron beam irradiator (Komenda, Slovenia) comprises two accelerators, providing irradiation in opposing vertical directions onto two under beam conveyors connected in series. Accelerator 1 provides radiation in a downward direction from above the conveyor system, Accelerator 2 is located underneath the conveyor system, providing radiation in an upward direction. The respirators irradiated to 10 kGy and 20 kGy were processed using a single electron accelerator from above and the respirators irradiated to 50 kGy were processed using one accelerator from above and one from below, each delivering 25 kGy. The delivered dose was measured using four termoiluminiscent detectors for each dose that were placed in close proximity to the irradiated samples. The accelerator specifications are shown in Table 3S.

2.9. Electrostatic properties

Electrostatic properties of samples were determined by measurements of surface potential, which is related to the surface charge density. A non-contact electrostatic voltmeter, model 542A (Trek, USA) was used to follow the surface potential using a measurement probe positioned at a distance of 20 mm from the sample surface. Complete filters consisting of four layers were considered for these measurements. The variation of the measured values of surface potential is mainly related to the heterogeneity of the analyzed masks. We analyzed three pieces of every FFR and an average value of the surface potential was calculated. A device for charge deposition (ZeroStat 3, Sigma Aldrich) was used to build up negative and positive potentials. Recharging was performed on the FFRs which were irradiated with gamma-rays and high energy electrons to the dose of 20 kGy. After recharging, the FFRs were again analyzed for filtration efficiency.

3. Results and discussion

The measured FFP2 and FFP3 respiratory masks were comprised of four layers. Only one of the layers acts as filter for measured particle diameters, with an overall particle removal efficiency (PRE) higher than 99% (Table 1S). Other layers act as support for the filter and may filter larger particles [23]. The PRE and surface potentials were measured before and after irradiation with gamma rays or electron-beam on three or four identical masks of each type. The non-irradiated masks had PRE values of 99.5% and 100% for FFP2 and FFP3, respectively. Both types of masks exhibited a negative surface potential before irradiation of −0.4 kV (FFP2) and −0.6 kV (FFP3). After irradiation, a decrease in PRE was observed, as well as the removal of almost all surface charge (Table 1). The PRE dropped by approximately 15% for the FFP2 and 10% for the FFP3, with no noticeable difference between various doses of ionizing radiation and methods of irradiation (Fig. 1 and 1S). The surface charge was almost completely removed at all doses, with the remained surface potential values between −190 V and +20 V. The results are in agreement with the results of previous reports [6–8] whereby the drop in PRE was attributed to the removal of surface charge. The 5% difference between the PRE of FFP2 and FFP3 is attributed to higher quality of the FFP3 filtering layer due to a different manufacturing process. As it can be seen from Fig. 9S–D and 10S-F, the FFP3 filtering layer has a larger amount of iPP fibres with smaller diameters. As it is described in Ref. [9], when the surface potential is removed, the main particle removal mechanism for particle diameters bellow 500 nm is interception due to diffusion of particles, which increases with the decreasing fibre diameter. The recharging yielded

Table 1
Average surface potential (SP) and particle removal efficiency (PRE) of FFP2 and FFP3 FFRs at different irradiation doses [24]. The quoted uncertainties represent the observed standard deviation. There is only one measurement of recharged FFRs presented in the table due to different SP values of each recharged FFRs. * - filters that were recharged with a negative surface potential, ** - filters that were recharged with a positive surface potential.

	Dose (kGy)	Surface Potential (kV)		Particle removal efficiency (%)	
		Gamma	E-beam	Gamma	E-beam
	0	-0.4 ± 0.1		$99.5^{+0.5}_{-0.9}$	
FFP2	10	$\|SP\| < 0.1$	$\|SP\| < 0.1$	83.4 ± 0.8	84 ± 2
	20	$\|SP\| < 0.1$	$\|SP\| < 0.1$	87 ± 10	82 ± 2
	50	-0.2 ± 0.2	$\|SP\| < 0.1$	87 ± 1	86 ± 4
	20*	-2.3 ± 0.3	-2.3 ± 0.3	99.4	98.7
	20**	2.1 ± 0.2	2.1 ± 0.2	98.5	97.9
	0	-0.6 ± 0.2		$100^{+0.0}_{-0.05}$	
FFP3	10	$\|SP\| < 0.1$	$\|SP\| < 0.1$	90 ± 2	92 ± 1
	20	$\|SP\| < 0.1$	$\|SP\| < 0.1$	91 ± 2	91 ± 1
	50	$\|SP\| < 0.1$	$\|SP\| < 0.1$	91 ± 2	91 ± 3
	20*	-2.8 ± 0.3	-2.2 ± 0.3	97.1	99.7
	20**	1.9 ± 0.2	1.9 ± 0.2	98.7	99.7

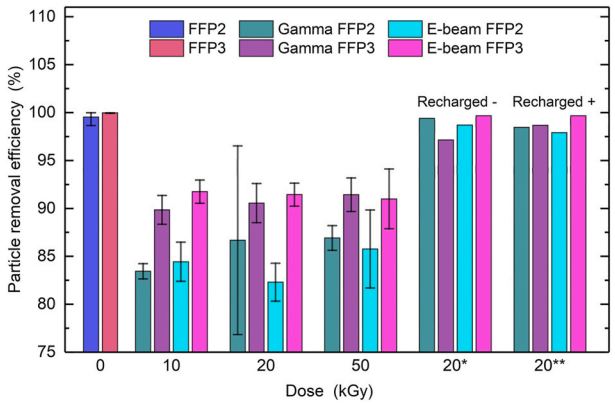

Fig. 1. Particle removal efficiency (PRE) as a function of the dose. Error bars represent the standard deviation. * - filters that were recharged with a negative surface potential, ** - filters that were recharged with a positive surface potential.

surface potential values of −2 kV to −3 kV for negative recharging and around +2 kV for positive recharging. Recharging increased the PRE in both filters, close to the values measured before irradiation (Table 1).

Fig. 2 shows the PRE values as a function of particle diameter for non-irradiated, gamma and e-beam irradiated FFRs at 20 kGy and the improved filtration efficiency of the recharged samples. The non-irradiated FFRs show adequate filtering efficiency for all measured particle sizes. Both types of irradiation decreased the PRE of the FFP3 FFRs up to 18% for particles larger than 25 nm, while in the case of FFP2 FFRs the PRE was reduced for 28% and 35% for e-beam and gamma-rays irradiated FFRs, respectively. The deviation of both curves is clearly visible for particles larger than 80 nm. After recharging, the overall PRE significantly increased for both types of FFRs irradiated by both methods. For particles below 80 nm in diameter, the filtering efficiency returns practically back to 100%, while for particles between 200 nm and 600 nm, the PRE is still lower compared to the non-irradiated filter, as seen in Fig. 2 and reported in Table S2. This is probably due to incomplete recharging of the filtrating layer, as the charge is applied only to the surface of the mask. As it is known, PRE is the lowest for particles between 50 nm and 500 nm [9]. In this range the particles are too large for diffusion to be an efficient removal mechanism, and too small for direct impaction or interception.

The electric field of the surface potential acts on aerosol particles by means of Coulomb forces or by dielectrophoretic forces. In the former,

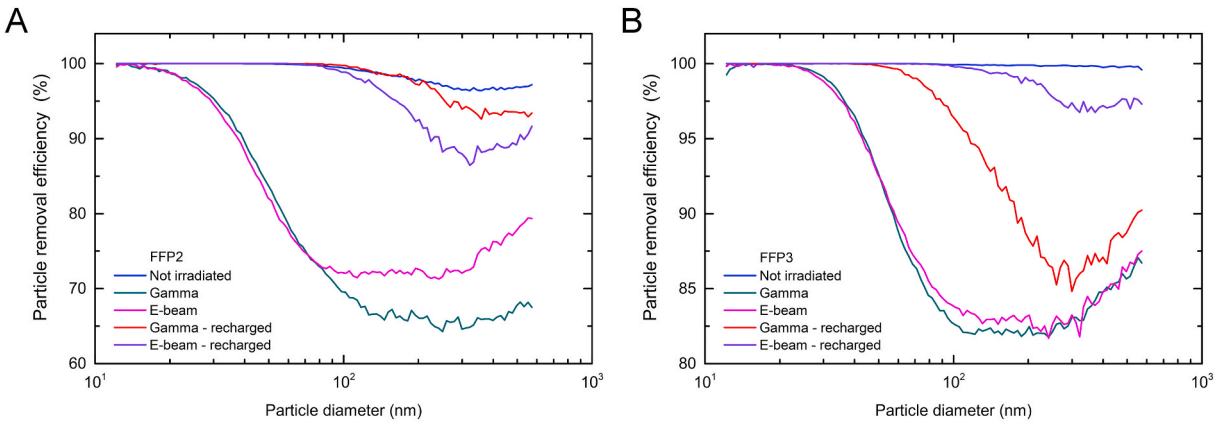

Fig. 2. Particle removal efficiency (PRE) as a function of particle diameter for: A) FFP2 and B) FFP3 FFRs. Non-irradiated FFRs (blue line) are compared with FFRs after exposure to 20 kGy gamma radiation (Gamma) and electron beam radiation (E-beam) before and after recharging with the negative charge. (For interpretation of the references to colour in this figure legend, the reader is referred to the Web version of this article.)

the opposite charges are attracted and similar charges are repelled, while in the latter the electric field induces an electric dipole in a dielectric particle. The spatial charges composing a dipole inside an aerosol particle are equal in magnitude, but due to the spatial variation of the electric field, the attractive force always prevails over the repulsive force. The dielectrophoretic forces have a shorter range and are smaller in magnitude compared to Coulomb forces with similar charge configurations [25,26]. Consequently, the PRE for neutral particles is lower than for charged particles [27]. As it turns out, most of the aerosol particles found in the environment possess electrostatic charge. The study of positively and negatively charged aerosol particles has shown only a weak dependency on particle removal efficiency between the two while using a charged filter [27]. In our study, the FFRs were recharged with a positive and negative charge, and the obtained PRE are similar in value in both cases.

A careful analysis shows that during the experiment the PRE varies with time. First, for all non-recharged filters, the PRE increased with time (on a timescale of 30 min), Fig. 2S. The reason is likely the accumulation of aerosol particles on the filters, which clog the mask and increase the filtering. The effect is most pronounced for particles larger 50 nm, Figs. 3S and 4S. In contrast, for recharged masks, the effect was the opposite, PRE decreased with time, indicating a loss of charge (perhaps due to recombination of reapplied charge due to charged dust particles). The overall PRE for the FFP2 FFRs did not drop significantly, while for the gamma ray irradiated FFP3 FFRs, the PRE decreased by 4%. As for the e-beam irradiated FFP3 FFRs, the PRE did not decrease with time, indicating that the filter performs as well as a non-irradiated one and negligible amount of charge is lost. It can be concluded that recharging the FFRs after irradiation/sterilization with ionizing radiation could be used in times when there is a shortage of FFRs. As the sterilization dose is applied within seconds/hours and the high throughput of modern electron beam/gamma ray sterilization facilities this method could be readily used during an emergency.

To evaluate any mechanical, morphological, and chemical changes on the irradiated masks, Raman spectroscopy, X-ray photoelectron spectroscopy (XPS), scanning electron microscopy (SEM), and dynamic mechanical analysis (DMA) were used.

Raman spectroscopy revealed that all layers in both FFP2 and FFP3 filters are made of isostatic polypropylene (iPP), Figs. 3 and 5S. Multiple spectra were taken on each layer, showing that the intensity varies within the layers. This is due to different iPP molecular chain orientations with respect to the laser polarization [28]. The peak at 1153 cm^{-1} suggests that all layers also contain some amorphous phase. Raman spectra of the irradiated filters are compared with the non-irradiated ones in Fig. 3. No peaks are missing and no peak shifts were observed, confirming that the iPP retains its crystal structure even after gamma-ray or e-beam irradiation [29,30]. Although some studies showed [31,32] that gamma-ray irradiation forms hydroxyl (OH) and carbonyl (C=O) groups on polymers such as iPP, we did not observe any peaks corresponding to these groups at any dose [33].

XPS spectra of carbon C 1s and oxygen O 1s on all filters were acquired in order to obtain insight into the surface chemistry of iPP filters before and after radiation exposure. Typical carbon C 1s spectra for FFP2 and FFP3 FFRs after 10 kGy exposure to gamma and e-beam radiation are shown in Fig. 4. The peaks in the spectra are located at the binding energy of 284.8 eV. The peaks are symmetrical, narrow (FWHM of 1.2

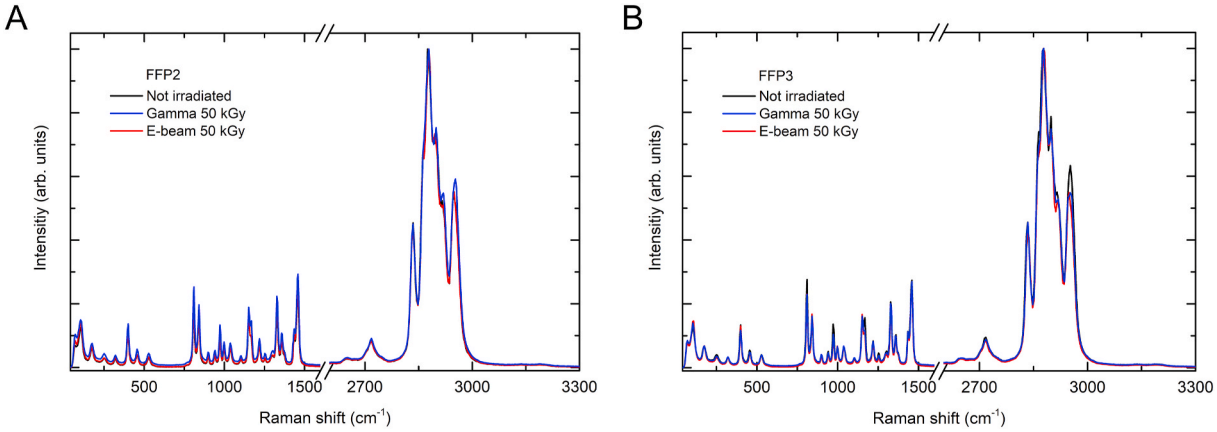

Fig. 3. Raman spectra of non-irradiated and irradiated filter layers at 50 kGy with gamma-ray and e-beam for A) FFP2 and B) FFP3 FFRs [24].

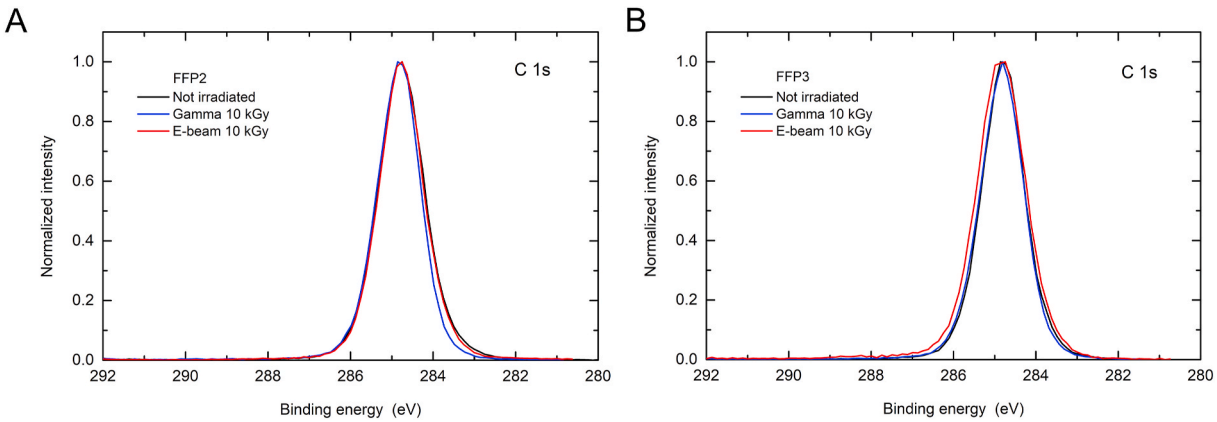

Fig. 4. XPS spectra of carbon C 1s from surfaces of filters in (a) FFP2 and (b) FFP3 FFRs before and after 10 kGy exposures to gamma and e-beam radiation [24].

eV), which is characteristic for C–C/C–H bonds present in the iPP polymer [34]. No additional peaks at the binding energy of 286 eV or higher were detected, which might be related to C–O, C–OH, O–C=O bonds formed on the surface during radiation exposure or adsorption of another species. There is minor broadening of the C 1s spectra at the low binding energy side which may be related to the charging of the iPP fabrics during XPS analysis. We should note that small oxygen O 1s peaks at 532 eV in XPS spectra were present on some iPP samples indicating the presence of oxygen-based molecules on the surface. The surface concentration of oxygen was calculated to be between 0 at. % and 0.3 at. % for fresh FFP2 and FFP3 samples and between 0.3 at. % and 0.7 at. % for all exposed samples. Due to the very low presence of oxygen and the absence of additional types of C-bonds on fibres, we assume that no chemical changes occurred on surface of filters during exposure. Therefore, the reduction of charge on filter materials after gamma and e-beam radiation is not related to changes in surface chemistry.

SEM images of non-irradiated layers reveal that both FFRs have supporting layers from iPP fibres with the diameters ranging from 10 μm up to 100 μm (Figs. 9S and 10S) while the layers with the highest PRE have substantially thinner fibres, ranging from 500 nm up to 10 μm (Fig. 5-A). Comparing SEM images before and after radiation we observed no substantial morphological changes in fibre structure. Some broken fibres were observed in the irradiated samples. However, the broken fibres are few and far between, therefore we cannot claim that the damage was caused solely by radiation but could as well be a consequence of handling and sample preparation. The changes of the mechanical properties are likely due to chemical changes (chain scissoring [30]) and cannot as such be seen from SEM images.

It is possible to conclude that irradiations did not cause substantial changes in fibres morphology. Particle accumulation on a single iPP fibre of a FFP3 FFR after the exposure to the aerosol during the PRE measurement is shown in Fig. 5-B.

Mechanical properties were analyzed with a DMA where the measured storage and loss moduli represent the elastic and viscous responses of the material, respectively. The storage moduli of the filtering layer of FFP2 and FFP3 FFRs are shown in Fig. 6. As the storage modulus of the FFP2 filtration layer is in the range of a few 100 MPa, the storage modulus of the FFP3 filtration layer is in the range of a few 10 MPa. It can be seen that in both cases the storage moduli decrease with temperature due to the increased segmental mobility of the polymer chains as one would expect for iPP [35]. The decrease in the storage moduli occurs between 0 °C and 20 °C, which is associated with the beta relaxation (glass-rubber transition) of amorphous polypropylene [35–37]. In the case of FFP2 FFRs the storage moduli of the gamma-ray irradiated samples decrease with increasing dose due to chain scissoring [30]. The 50 kGy sample could not be measured as it was so brittle that it disintegrated upon extraction from the surrounding layers. Also, all e-beam irradiated samples have a lower storage modulus than the non-irradiated one, with the 20 kGy sample having a slightly higher overall storage modulus than the 10 kGy. The 50 kGy sample could still be measured but the storage modulus decreased by almost 75%. The loss modulus also decreases with temperature and has no apparent peak at the glass-rubber transition which is reflected in a monotone Tan delta plot, Fig. 8S. The same observations regarding the storage and loss modulus apply also for the FFP3 filtration layer.

4. Conclusions

The acute shortages of personal protection equipment during the COVID-19 forced health workers and other workers using FFRs to

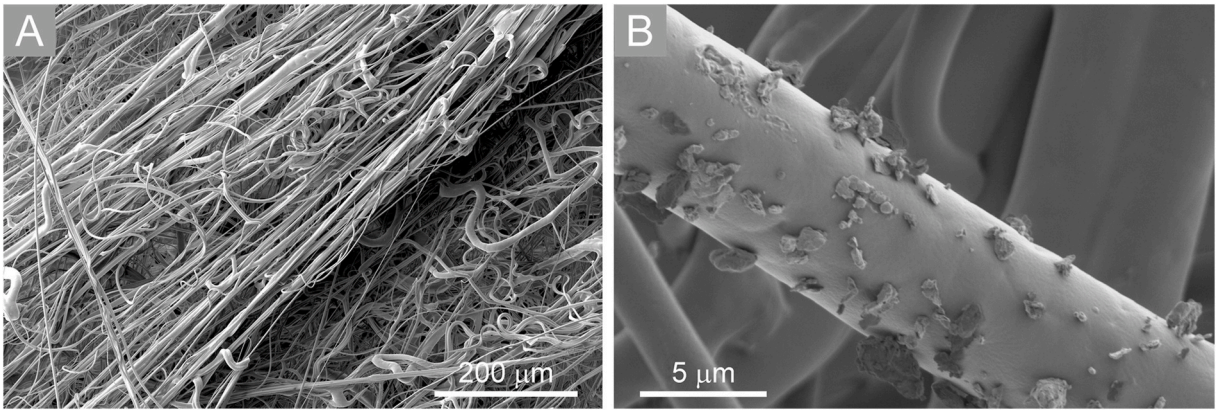

Fig. 5. A) SEM images of the filtrating layer of non-irradiated FFP3 FFRs; B) Particle accumulation on an iPP fibre in a FFP3 FFR after exposure to aerosol powder.

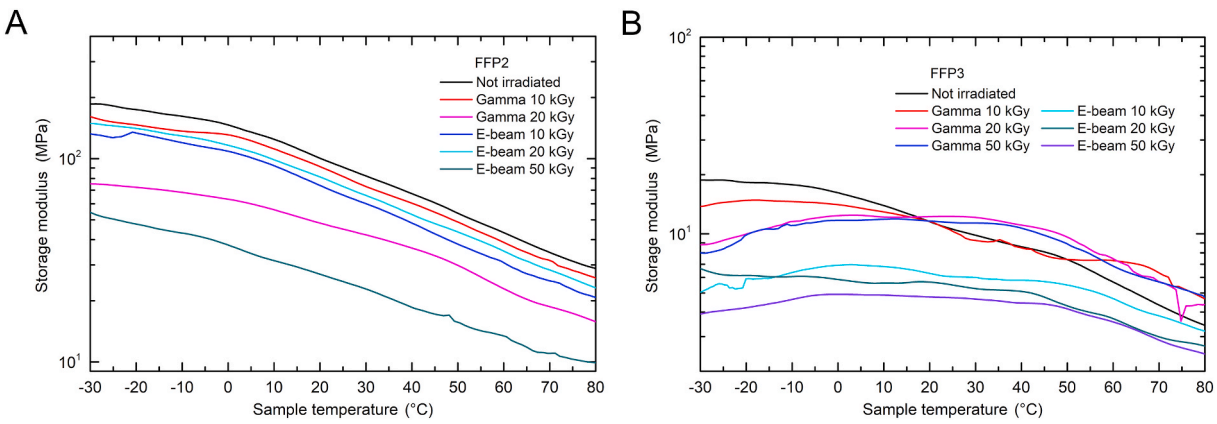

Fig. 6. Storage modulus of A) FFP2 and B) FFP3 FFRs before and after the irradiation with gamma-rays or electron-beam.

explore various strategies of recycling single-use respirators. In this study we investigated the sterilization of FFP2 and FFP3 respirators using ionizing radiation, namely gamma and electron beam irradiation. We performed a structural, chemical, mechanical and filtration analysis with the aim to provide an overview of the effects of the irradiation on the material and on the respirator filtration characteristics.

Our results demonstrate that both types of irradiation remove the surface charge from the filtering layer of the respirators, which results in a decrease of the particle removal efficiency of 10% for FFP3 and 15% for FFP2 FFRs – as the electrostatic attraction between the particles and the polypropylene fibres is one of the main mechanisms of particle filtering below 500 nm. We demonstrate that by reapplying charge to the filtering layer, either positive or negative, the filtration performance in almost all cases returns to that of the original FFR.

Irradiation is thus a viable method for sterilization of respirators. The chemical structure of the fabric did not change due to irradiation, while the mechanical integrity of the material deteriorated only when exposed to highest doses (50 kGy). While not practical for individual use, or use in smaller hospitals, this sterilization approach may in principle be possible for large-scale use, in dedicated facilities that deal with sterilization of medical equipment, provided that the charge is reapplied to the respirator afterwards with conventional methods. The number of sterilizations is limited by the material properties. Our measurements indicate that the sterilization up to two times is possible before the mechanical degradation renders the respirator unsafe for further use.

CRediT authorship contribution statement

Luka Pirker: Methodology, Formal analysis, Data curation, Writing - review & editing. **Anja Pogačnik Krajnc:** Data curation, Writing - review & editing, Visualization, Validation. **Jan Malec:** Conceptualization, Methodology, Writing - original draft, Project administration. **Vladimir Radulović:** Methodology, Formal analysis, Resources. **Anton Gradišek:** Conceptualization, Investigation, Writing - review & editing. **Andreja Jelen:** Resources, Data curation. **Maja Remškar:** Supervision, Funding acquisition, Writing - review & editing. **Igor B. Mekjavić:** Supervision, Funding acquisition. **Janez Kovač:** Resources, Formal analysis. **Miran Mozetič:** Writing - review & editing. **Luka Snoj:** Conceptualization, Supervision, Project administration, Funding acquisition, Writing - review & editing.

Declaration of competing interest

The authors declare that they have no known competing financial interests or personal relationships that could have appeared to influence the work reported in this paper.

Acknowledgement

The authors acknowledge the financial support from the Slovenian Research Agency (research core funding No. P2-0073 Reactor Physics, P2-0209 Artificial intelligence and intelligent systems, P1-0099 Physics of soft matter, surfaces, and nanostructures, P1-0125 Magnetic resonance and dielectric spectroscopy of smart new materials, P2-0076 Automation, robotics and biocybernetics and P2-0082 Thin-film structures and plasma surface engineering). We would like to thank CENN Nanocenter for the use of FIB, Helios NanoLab. Special thanks go to the operators of the TRIGA Mark II reactor in Ljubljana who have supported the development by irradiating the respirators in the reactor and the Government of Slovenia and the Slovenian Ministry of Health for donating the FFP2 and FFP3 respirators used in the research.

Appendix A. Supplementary data

Supplementary data to this article can be found online at https://doi.org/10.1016/j.memsci.2020.118756.

References

[1] K. O'Hearn, et al., 'Efficacy and Safety of Disinfectants for Decontamination of N95 and SN95 Filtering Facepiece Respirators: A Systematic Review', Open Science Framework, Apr. 2020, https://doi.org/10.31219/osf.io/ct6m8 preprint.
[2] D.J. Viscusi, M.S. Bergman, B.C. Eimer, R.E. Shaffer, Evaluation of five decontamination methods for filtering facepiece respirators, Ann. Occup. Hyg. 53 (8) (Nov. 2009) 815–827, https://doi.org/10.1093/annhyg/mep070.
[3] Can N95 respirators Be reused after disinfection? How many times? ACS Nano', 2020. https://pubs.acs.org/doi/10.1021/acsnano.0c03597. (Accessed 29 May 2020). accessed.
[4] E. Hossain, S. Bhadra, H. Jain, A. Bhattacharya, S. Ghosh, D. Levine, Recharging Improves Efficiency of Decontaminated N95 Masks, Accessed, ArXiv200413641 Phys., Apr. 2020 [Online]. Available: http://arxiv.org/abs/2004.13641. (Accessed 30 May 2020).
[5] P.S.C. Juang, P. Tsai, N95 respirator cleaning and reuse methods proposed by the inventor of the N95 mask material, *J. Emerg. Med.*, Apr (2020), https://doi.org/10.1016/j.jemermed.2020.04.036.
[6] L. Cortella et al., 'FEASIBILITY OF GAMMA OR E-BEAM IRRADIATION AS A TREATMENT FOR REUSE OF MEDICAL MASKS AFTER A FIRST USE', IAEA.
[7] J. M. Yun et al., 'reportA Report for Sterilizing Personal Protective Equipment by Ionizing Radiation', IAEA.
[8] A. Cramer, et al., Disposable N95 masks pass qualitative fit-test but have decreased filtration efficiency after cobalt-60 gamma irradiation, medRxiv (2020), https://doi.org/10.1101/2020.03.28.20043471.
[9] Aerosol Technology, Properties, behavior, and measurement of airborne particles, in: Wiley', Wiley.Com, second ed., 2020 (accessed Jun. 09, 2020).
[10] N. Chen, et al., Epidemiological and clinical characteristics of 99 cases of 2019 novel coronavirus pneumonia in Wuhan, China: a descriptive study, Lancet 395 (10223) (Feb. 2020) 507–513, https://doi.org/10.1016/S0140-6736(20)30211-7.
[11] S. Cheng, et al., Effect of temperature on the structure and filtration performance of polypropylene melt-blown nonwovens, Autex Res. J. 1 (2020) ahead-of-print.
[12] T. Miki, M. Ikeya, Theoretical response of electret dosimeter to ionizing radiation, Jpn. J. Appl. Phys. 24 (4R) (Apr. 1985) 496, https://doi.org/10.1143/JJAP.24.496.

[13] G.M. Sessler, Bernhard Gross and the evolution of modern electret research, Braz. J. Phys. 29 (2) (Jun. 1999) 220–225, https://doi.org/10.1590/S0103-97331999000200003.
[14] A.G. Kravtsov, S.V. Zotov, H. Brunig, Peculiarities of the electret state of melt-spun and melt-blown fibrous polypropylene materials, Mech. Compos. Mater. 36 (Nov. 2000) 491–496, https://doi.org/10.1023/A:1006762701365.
[15] Kubik D.A., Davis C.I., Melt-blown fibrous electrets', US Patent 4,215,682 (Aug. 05, 1980).
[16] E.R. Frederick, Some effects of electrostatic charges in fabric filtration, J. Air Pollut. Contr. Assoc. 24 (12) (Dec. 1974) 1164–1168, https://doi.org/10.1080/00022470.1974.10470030.
[17] R.N. Work, R.D. McCammon, R.G. Saba, Effective dipole moment of polypropylene, J. Chem. Phys. 41 (9) (Nov. 1964) 2950–2951, https://doi.org/10.1063/1.1726384.
[18] F. Feldmann, W.L. Shupert, E. Haddock, B. Twardoski, H. Feldmann, Gamma irradiation as an effective method for inactivation of emerging viral pathogens, Am. J. Trop. Med. Hyg. 100 (5) (2019) 1275–1277, https://doi.org/10.4269/ajtmh.18-0937.
[19] Standard EN 149:2001+A1, Respiratory Protective Devices - Filtering Half Masks to Protect against Particles - Requirements, Testing, Marking, European Committee for Standardization, 2009 [Online]. Available: May 2009, https://standards.cen.eu/dyn/www/f?p=204:110:0FSP_PROJECT,FSP_ORG_ID:32928,6062&cs=1FC98AD34A5EE26A0CB5A6155ED4D6E5E.
[20] A. Gruel, K. Ambrožič, C. Destouches, V. Radulović, A. Sardet, L. Snoj, Gamma-heating and gamma flux measurements in the JSI TRIGA reactor: results and prospects, IEEE Trans. Nucl. Sci. 67 (4) (Apr. 2020) 559–567, https://doi.org/10.1109/TNS.2020.2974968.
[21] Delayed gamma determination at the JSI TRIGA reactor by synchronous measurements with fission and ionization chambers, Nucl. Instrum. Methods Phys. Res. Sect. Accel. Spectrometers Detect. Assoc. Equip. 911 (Dec. 2018) 94–103, https://doi.org/10.1016/j.nima.2018.09.103.
[22] K. Ambrožič, G. Žerovnik, L. Snoj, Computational analysis of the dose rates at JSI TRIGA reactor irradiation facilities, Appl. Radiat. Isot. 130 (Dec. 2017) 140–152, https://doi.org/10.1016/j.apradiso.2017.09.022.
[23] S.R. Lustig, et al., Effectiveness of common fabrics to block Aqueous aerosols of virus-like nanoparticles, ACS Nano (May 2020), https://doi.org/10.1021/acsnano.0c03972.
[24] J. Malec et al., 'Respirator sterilization raw data', vol. 1, doi: 10.17632/tf62c3ckhr.1.
[25] R. Brown, Effect of electric charge in filter materials, Filtr. Sep. 26 (1) (Jan. 1989) 46–51, https://doi.org/10.1016/S0015-1882(89)80057-6.
[26] Q. Sun, W.W.-F. Leung, Charged PVDF multi-layer filters with enhanced filtration performance for filtering nano-aerosols, Separ. Purif. Technol. 212 (Apr. 2019) 854–876, https://doi.org/10.1016/j.seppur.2018.11.063.
[27] Deposition and resuspension of selected aerosols particles on electrically charged filter materials for respiratory protective devices. https://reference.medscape.com/medline/abstract/16329780. (Accessed 24 August 2020) accessed.
[28] M. Arruebarrena de Báez, P.J. Hendra, M. Judkins, The Raman spectra of oriented isotactic polypropylene, Spectrochim. Acta. A. Mol. Biomol. Spectrosc. 51 (12) (Nov. 1995) 2117–2124, https://doi.org/10.1016/0584-8539(95)01512-1.
[29] R. Mishra, et al., Electron induced modification in polypropylene, Radiat. Meas. 33 (6) (Dec. 2001) 845–850, https://doi.org/10.1016/S1350-4487(01)00038-5.
[30] S.A.S. Alariqi, A.P. Kumar, B.S.M. Rao, R.P. Singh, Effect of γ-dose rate on crystallinity and morphological changes of γ-sterilized biomedical polypropylene, Polym. Degrad. Stabil. 94 (2) (Feb. 2009) 272–277, https://doi.org/10.1016/j.polymdegradstab.2008.10.027.
[31] J. Lacoste, D. Vaillant, D.J. Carlsson, Gamma-, photo-, and thermally-initiated oxidation of isotactic polypropylene, J. Polym. Sci. Part Polym. Chem. 31 (3) (1993) 715–722, https://doi.org/10.1002/pola.1993.080310316.
[32] P.V. Vardhan, L.I. Shukla, FT-IR investigations on effect of high doses of gamma radiation-induced damage to polystyrene and mechanism of formation of radiolysis products, Radiat. Environ. Biophys. 57 (3) (2018) 301–310, https://doi.org/10.1007/s00411-018-0740-y.
[33] J. Karger-Kocsis (Ed.), Polypropylene: an A-Z Reference, Springer Netherlands, 1999.
[34] I. Junkar, et al., Plasma treatment-promising tool for preparation of disposable monolithic columns, J. Anal. Bioanal. Tech. 6 (4) (2015) 1.
[35] S.M.L. Rosa, S.M.B. Nachtigall, C.A. Ferreira, Thermal and dynamic-mechanical characterization of rice-husk filled polypropylene composites, Macromol. Res. 17 (1) (Jan. 2009) 8–13, https://doi.org/10.1007/BF03218594.
[36] E. Passaglia, G.M. Martin, Dependence of mechanical relaxation on morphology in isotactic polypropylene, J. Res. Natl. Bur. Stand. Sect. Phys. Chem. 68A (5) (1964) 519–527, https://doi.org/10.6028/jres.068A.049.
[37] A.S. Luyt, M.D. Dramićanin, Ž. Antić, V. Djoković, Morphology, mechanical and thermal properties of composites of polypropylene and nanostructured wollastonite filler, Polym. Test. 28 (3) (May 2009) 348–356, https://doi.org/10.1016/j.polymertesting.2009.01.010.